ЖЭТФ, 2015, том 148, вып. 4 (10), стр. 696–705

MAGNETIC PROPERTIES OF THE SPIN-3/2 BLUME–CAPEL MODEL ON A HEXAGONAL ISING NANOWIRE

Y. Kocakaplan [a], ***M. Ertaş*** [b*]

[a] *Graduate School of Natural and Applied Sciences, Erciyes University 38039, Kayseri, Turkey*

[b] *Department of Physics, Erciyes University 38039, Kayseri, Turkey*

Received December 18, 2014

Magnetic properties, such as magnetizations, internal energy, specific heat, entropy, Helmholtz free energy, and phase diagrams of the spin-3/2 Blume–Capel model on a hexagonal Ising nanowire with core–shell structure are studied by using the effective-field theory with correlations. The hysteresis behaviors of the system are also investigated and the effects of Hamiltonian parameters on hysteresis behaviors are discussed in detail. The obtained results are compared with some theoretical results and a qualitatively good agreement is found.

DOI: 10.7868/S0044451015100065

1. INTRODUCTION

The Blume–Capel model is a spin-1 Ising model with a bilinear (J) and a single-ion (D) potential that was originally proposed by Blume [1] and Capel [2] independently to study magnetic systems. The spin-3/2 Ising system was first introduced in [3], as long ago as 1972, to explain magnetic and crystallographic phase transitions in some rare-earth compounds such as $DyVO_4$ [4, 5], and then extended to describe tricritical properties in ternary fluid mixtures (ethanol–water–carbon–dioxide) [6]. Among various spin Ising systems, the spin-3/2 Ising system has gained much attention in the last years, and although the model was introduced about 40 years ago, its equilibrium behaviors are still actively investigated, with different effects being considered. Many methods have been used in discussing the equilibrium properties of the spin-3/2 Ising system, such as the effective field theory with corrections (EFT) [7–10], the cluster variation method [11], Monte Carlo (MC) simulation [12, 13], renormalization group technique [14], and mean-field theory (MFT) [15–17], and so on.

On the other hand, it is well known that splendid and enormous achievements in the technologies and experimental techniques have recently enabled the production of nanostructures such as nanotubes, nanowires, nanocubes, nanorods, etc. Theoretically, magnetic properties of magnetic behaviors of the spin-1/2 or spin-1 nanostructure Ising system have been investigated successfully by adopting a core–shell structure of the Ising systems. They have been investigated by means of various techniques such as MFT, EFT with correlations, MC simulations, etc. (see [18–29] and the references therein). Moreover, some dynamic magnetic properties of nanostructure Ising systems have been investigated for spin-1/2 or spin-1 [30–33].

Despite these studies, the equilibrium properties of the nanostructure Ising systems have not been investigated equally thoroughly for higher-spin models; there has been only one investigation, to our knowledge, of the equilibrium properties of the nanostructures with a higher spin. In this study [34], hysteresis and compensation behaviors of the spin-3/2 cylindrical Ising nanotube system are studied in the framework of the EFT with correlations. The effects of the Hamiltonian parameters are investigated on the magnetic and thermodynamic quantities, such as the total magnetization, hysteresis curves, and compensation behaviors of the system. Hence, further effort should be invested into studying the equilibrium properties of higher-spin nanostructures. The purpose of this paper is to investigate magnetic properties (magnetizations, internal energy, specific heat, entropy, and Helmholtz free energy) and phase diagrams of the spin-3/2 Blume–Ca-

*E-mail: mehmetertas@erciyes.edu.tr

pel model on a hexagonal Ising nanowire (HIN) with a core–shell structure by using the EFT with correlations. We also mention that the EFT method, without introducing mathematical complexity, can incorporate some effects of spin–spin correlations through the use of the Van der Waerden identities and provide results that are quite superior to those obtained using the MFT. Therefore, the magnetic behavior of different Ising systems has been studied (see [35–38] and the references therein) via the EFT with correlation in recent years. Moreover, the theory is used to investigate main physical characteristics of one-dimensional objects [39]. In this study, the effects of the next-nearest-neighbor exchange interaction on the magnetic properties were investigated in the one-dimensional Ising system by using the EFT with correlation.

The outline of this paper is as follows. In Sec. 2, the EFT formalism is presented briefly. The detailed numerical results and discussions are given in Sec. 3. Finally, Sec. 4 is devoted to a summary and conclusion.

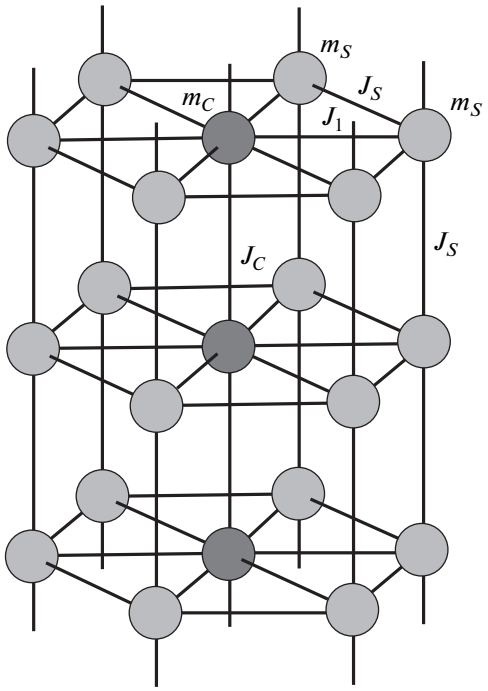

Fig. 1. Schematic representation of a hexagonal Ising nanowire. The respective grey (blue) and black (red) spheres indicate magnetic atoms at the surface shell and core. (Color online see arXiv:1406.6537)

2. FORMALISM

The Hamiltonian of the spin-3/2 HIN system, including nearest-neighbor interactions and the crystal field, is given by

$$H = -J_S \sum_{\langle ij \rangle} S_i S_j - J_C \sum_{\langle mn \rangle} S_m S_n - J_1 \sum_{\langle im \rangle} S_i S_m - D\left(\sum_i S_i^2 + \sum_m S_m^2\right) - h\left(\sum_i S_i + \sum_m S_m\right), \quad (1)$$

where each S_i can take the values $\pm 3/2$ and $\pm 1/2$ and $\langle \ldots \rangle$ detones summation over all pairs of nearest-neighbor sites. The exchange interaction parameters J_S, J_C, and J_1 are respective interactions between two nearest-neighbor magnetic atoms in the shell, in the core, and between the shell and core (see Fig. 1). D stands for the single-ion anisotropy and h is the external magnetic field.

The problem is to evaluate the means $\langle S_i \rangle$, $\langle S_m \rangle$, $\langle S_i^2 \rangle$, $\langle S_m^2 \rangle$, $\langle S_i^3 \rangle$, and $\langle S_m^3 \rangle$. The starting point for statistics of the present spin system is the exact relation due to Callen [40]:

$$\langle S_{i,j,m}^k \rangle = \left\langle \prod_\delta \{A(\alpha) + B(\alpha) S_{i,j,m+\delta} + C(\alpha) S_{i,j,m+\delta}^2 + D(\alpha) S_{i,j,m+\delta}^3\} \right\rangle F_k(x)|_{x=0}, \quad (2)$$

where $\alpha = J_x \nabla$ ($J_x = J_1$, J_C, or J_S) and δ denotes the nearest-neighbor sites of the central site i (or a site j, m); $\nabla = \partial/\partial x$ is a differential operator. Expression (2) is also exact and is valid for any lattice. As discussed in Refs. [41–46], for the evaluation of mean values, we can use the exact Ising spin identities and the differential operator technique introduced in [47] and in [48], which is a more advanced method dealing with Ising systems than the MFT, because it includes more correlations. In the framework of the EFT with correlations, it is easy to find the magnetizations M_S and M_C, the quadruple moments q_S and q_C, and the octupolar moments r_S and r_C from coupled equations for the cylindrical spin-3/2 HIN system depicted in Fig. 1:

$$M_S = \langle S_i \rangle = \left[a_0 + a_1 \langle S_i \rangle + a_2 \langle S_i^2 \rangle + a_3 \langle S_i^3 \rangle\right]^4 \times \left[b_0 + b_1 \langle S_m \rangle + b_2 \langle S_m^2 \rangle + b_3 \langle S_m^3 \rangle\right] F_1(x+h)\big|_{x=0}, \quad (3a)$$

$$M_C = \langle S_m \rangle = \left[c_0 + c_1 \langle S_m \rangle + c_2 \langle S_m^2 \rangle + c_3 \langle S_m^3 \rangle\right]^2 \times \left[b_0 + b_1 \langle S_i \rangle + b_2 \langle S_i^2 \rangle + b_3 \langle S_i^3 \rangle\right]^6 F_1(x+h)\Big|_{x=0}, \quad (3b)$$

$$q_S = \langle S_i^2\rangle = \left[a_0 + a_1\langle S_i\rangle + a_2\langle S_i^2\rangle + a_3\langle S_i^3\rangle\right]^4 \times \times \left[b_0{+}b_1\langle S_m\rangle{+}b_2\langle S_m^2\rangle{+}b_3\langle S_m^3\rangle\right] F_2(x{+}h)\big|_{x=0}, \quad (4a)$$

$$q_C = \langle S_m^2\rangle = \left[c_0 + c_1\langle S_m\rangle + c_2\langle S_m^2\rangle + c_3\langle S_m^3\rangle\right]^2 \times \times \left[b_0{+}b_1\langle S_i\rangle{+}b_2\langle S_i^2\rangle{+}b_3\langle S_i^3\rangle\right]^6 F_2(x{+}h)\Big|_{x=0}, \quad (4b)$$

$$r_S = \langle S_i^3\rangle = \left[a_0 + a_1\langle S_i\rangle + a_2\langle S_i^2\rangle + a_3\langle S_i^3\rangle\right]^4 \times \times \left[b_0{+}b_1\langle S_m\rangle{+}b_2\langle S_m^2\rangle{+}b_3\langle S_m^3\rangle\right] F_3(x{+}h)\big|_{x=0}, \quad (5a)$$

$$r_C = \langle S_m^3\rangle = \left[c_0{+}c_1\langle S_m\rangle{+}c_2\langle S_m^2\rangle{+}c_3\langle S_m^3\rangle\right]^2 \times \times \left[b_0{+}b_1\langle S_i\rangle{+}b_2\langle S_i^2\rangle{+}b_3\langle S_i^3\rangle\right]^6 F_3(x{+}h)\Big|_{x=0}, \quad (5b)$$

where a_i, b_i, and c_i are the Van der Waerden coefficients given by

$$\begin{aligned} a_0 &= \frac{1}{8}\left(9\,\mathrm{ch}\left(\frac{1}{2}J_S\nabla\right) - \mathrm{ch}\left(\frac{3}{2}J_S\nabla\right)\right),\\ a_1 &= \frac{1}{12}\left(27\,\mathrm{sh}\left(\frac{1}{2}J_S\nabla\right) - \mathrm{sh}\left(\frac{3}{2}J_S\nabla\right)\right),\\ a_2 &= \frac{1}{2}\left(-\mathrm{ch}\left(\frac{1}{2}J_S\nabla\right) + \mathrm{ch}\left(\frac{3}{2}J_S\nabla\right)\right),\\ a_3 &= \frac{1}{12}\left(-3\,\mathrm{sh}\left(\frac{1}{2}J_S\nabla\right) + \mathrm{sh}\left(\frac{3}{2}J_S\nabla\right)\right), \end{aligned} \quad (6a)$$

$$\begin{aligned} b_0 &= \frac{1}{8}\left(9\,\mathrm{ch}\left(\frac{1}{2}J_1\nabla\right) - \mathrm{ch}\left(\frac{3}{2}J_1\nabla\right)\right),\\ b_1 &= \frac{1}{12}\left(27\,\mathrm{sh}\left(\frac{1}{2}J_1\nabla\right) - \mathrm{sh}\left(\frac{3}{2}J_1\nabla\right)\right),\\ b_2 &= \frac{1}{2}\left(-\mathrm{ch}\left(\frac{1}{2}J_1\nabla\right) + \mathrm{ch}\left(\frac{3}{2}J_1\nabla\right)\right),\\ b_3 &= \frac{1}{12}\left(-3\,\mathrm{sh}\left(\frac{1}{2}J_1\nabla\right) + \mathrm{sh}\left(\frac{3}{2}J_1\nabla\right)\right), \end{aligned} \quad (6b)$$

$$\begin{aligned} c_0 &= \frac{1}{8}\left(9\,\mathrm{ch}\left(\frac{1}{2}J_C\nabla\right) - \mathrm{ch}\left(\frac{3}{2}J_C\nabla\right)\right),\\ c_1 &= \frac{1}{12}\left(27\,\mathrm{sh}\left(\frac{1}{2}J_C\nabla\right) - \mathrm{sh}\left(\frac{3}{2}J_C\nabla\right)\right),\\ c_2 &= \frac{1}{2}\left(-\mathrm{ch}\left(\frac{1}{2}J_C\nabla\right) + \mathrm{ch}\left(\frac{3}{2}J_C\nabla\right)\right),\\ c_3 &= \frac{1}{12}\left(-3\,\mathrm{sh}\left(\frac{1}{2}J_C\nabla\right) + \mathrm{sh}\left(\frac{3}{2}J_C\nabla\right)\right). \end{aligned} \quad (6c)$$

The functions $F_1(x)$, $F_2(x)$, and $F_3(x)$ in Eqs. (3)–(5) are given as

$$F_1(x+h) = \frac{1}{2} \times \times \frac{3\,\mathrm{sh}\left[3\beta(x{+}h)/2\right] + \mathrm{sh}\left[\beta(x+h)/2\right]\exp(-2\beta D)}{\mathrm{ch}\left[3\beta(x{+}h)/2\right] + \mathrm{ch}\left[\beta(x+h)/2\right]\exp(-2\beta D)}, \quad (7a)$$

$$F_2(x+h) = \frac{1}{2} \times \times \frac{9\,\mathrm{ch}\left[3\beta(x{+}h)/2\right] + \mathrm{ch}\left[\beta(x{+}h)/2\right]\exp(-2\beta D)}{2\,\mathrm{ch}\left[3\beta(x{+}h)/2\right] + 2\,\mathrm{ch}\left[\beta(x{+}h)/2\right]\exp(-2\beta D)}, \quad (7b)$$

$$F_3(x+h) = \frac{1}{2} \times \times \frac{27\,\mathrm{sh}\left[3\beta(x{+}h)/2\right] + \mathrm{sh}\left[\beta(x{+}h)/2\right]\exp(-2\beta D)}{4\,\mathrm{ch}\left[3\beta(x{+}h)/2\right] + 4\,\mathrm{ch}\left[\beta(x{+}h)/2\right]\exp(-2\beta D)}. \quad (7c)$$

Here, $\beta = 1/k_BT$, T is the absolute temperature, k_B is the Boltzmann constant, and $k_B = 1.0$ throughout the paper. Equations (3)–(5) are also exact and are valid for any lattice. If we try to exactly treat all the spin–spin correlations for that equation, the problem rapidly becomes intractable. A first obvious attempt to deal with it is to ignore the correlations; the decoupling approximation is given by

$$\langle S_i S_{i'} \ldots S_{i^n}\rangle \approx \langle S_i\rangle\langle S_{i'}\rangle \ldots \langle S_{i^n}\rangle, \quad (8a)$$

$$\langle S_m S_{m'} \ldots S_{m^n}\rangle \approx \langle S_m\rangle\langle S_{m'}\rangle \ldots \langle S_{m^n}\rangle, \quad (8b)$$

with $i \neq i' \neq \ldots \neq i^n$ and $m \neq m' \neq \ldots \neq m^n$ introduced within the EFT with correlations. In fact, the approximation corresponds essentially to the Zernike approximation [49] in the bulk problem, and has been successfully applied to a great number of magnetic systems including surface problems [50, 51].

Using the definitions of the magnetizations in Eqs. (3a) and (3b), we can determine the total magnetization M_T of each site from Fig. 2*a* as

$$M_T = \frac{1}{7}(6M_S + M_C). \quad (9)$$

We also mention that we do not examine the thermal behaviors of q_S, q_C, r_S, and r_C because our Hamiltonian does not contain the biquadratic exchange interaction parameter, as can be seen in Eq. (1). However, we need Eqs. (3a) and (3b) to determine the behaviors of M_S and M_C.

The internal energy per site of the system can be calculated as

$$\frac{U}{N} = -\frac{1}{2}\left(\langle U_C\rangle + \langle U_S\rangle\right) - D\left(\langle q_C\rangle + \langle q_S\rangle\right) - - h\left(\langle m_C\rangle + \langle m_S\rangle\right), \quad (10)$$

where

$$U_C = \frac{\partial}{\partial\nabla}\left[c_0 + c_1\langle S_m\rangle + c_2\langle S_m\rangle^2 + c_3\langle S_m\rangle^3\right]^2 \times \times \left[b_0 + b_1\langle S_i\rangle + b_2\langle S_i\rangle^2 + b_3\langle S_i\rangle^3\right]^6 \times \times F_1(x+h)\big|_{x=0}, \quad (11a)$$

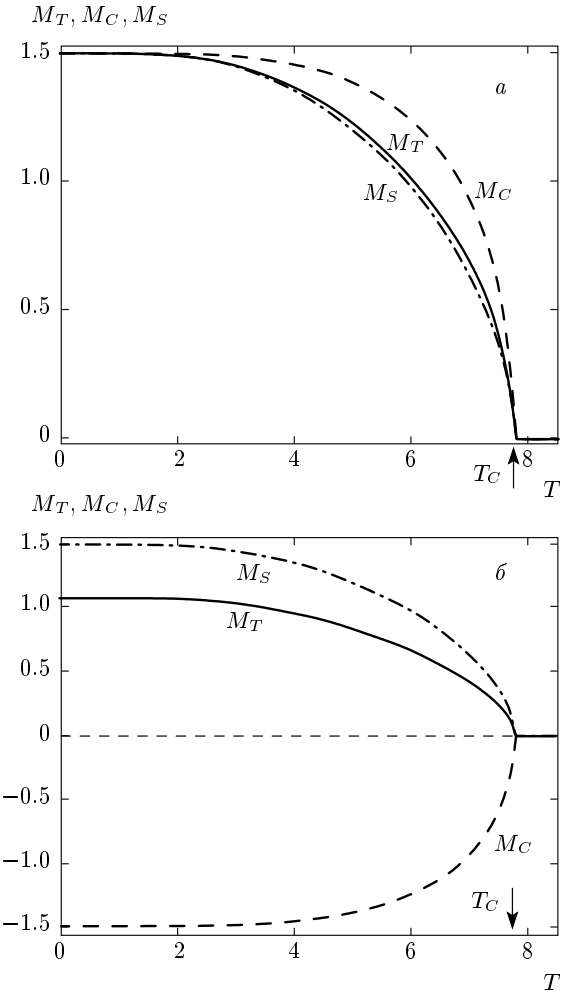

Fig. 2. Thermal variations of the magnetizations. (*a*) $J_1 = 1.0$, $J_C = 1.0$, $J_S = 1.0$, and $D = 1.0$. (*b*) $J_1 = -1.0$, $J_C = 1.0$, $J_S = 1.0$, and $D = 1.0$. (Color online see arXiv:1406.6537)

$$U_S = \frac{\partial}{\partial \nabla}\left[a_0 + a_1\langle S_i\rangle + a_2\langle S_i\rangle^2 + a_3\langle S_i\rangle^3\right]^4 \times \\ \times \left[b_0 + b_1\langle S_m\rangle + b_2\langle S_m\rangle^2 + b_3\langle S_m\rangle^3\right] \times \\ \times F_1(x+h)\big|_{x=0}. \quad (11b)$$

The specific heat of the system can be obtained from the relation

$$C_h = \left(\frac{\partial U}{\partial T}\right)_h. \quad (12)$$

The Helmholtz free energy of the system can be defined as

$$F = U - TS, \quad (13)$$

which, according to the third law of thermodynamics, can be written in the form

$$F = U - T\int_0^T \frac{C}{T}\,dT'. \quad (14)$$

The second term in the right-hand side of Eq. (14) is the entropy of the system according to the second law of thermodynamics.

3. NUMERICAL RESULTS AND DISCUSSIONS

In this section, our attention is focused on the study of the magnetic properties, the phase diagrams, and hysteresis behavior of a spin-3/2 HIN system with a core–shell structure.

3.1. Magnetic properties

3.1.1. Magnetizations

In Fig. 2, we investigated the thermal behavior of the total (M_T), core (M_C), and shell (M_S) magnetizations in both ferromagnetic ($J_1 > 0$) and antiferromagnetic ($J_1 < 0$) cases. This study leads us to characterizing the transitions and obtaining the transition points. For ferromagnetic and antiferromagnetic cases, a few explanatory examples are plotted in Fig. 2 to illustrate the calculation of the critical points as well as variation of magnetizations. Figure 2*a* is obtained for $J_1 = 1.0$, $J_C = 1.0$, $J_S = 1.0$, and $D = 1.0$. In Fig. 2*a*, the magnetizations M_T, M_S, and M_C decrease continuously with an increasing in the values of temperature below the critical temperature, and they vanish at $T_C = 7.85$; hence, a second-order phase transition occurs. The transition is from the ferromagnetic-3/2 ($F_{3/2}$) phase to the P phase. Figure 2*b* is obtained for $J_1 = -1.0$, $J_C = 1.0$, $J_S = 1.0$, and $D = 1.0$. In Fig. 2*b*, the magnetizations M_T and M_S decrease and M_C increases continuously with an increasing in the values of temperature below the critical temperature, and they vanish at $T_C = 7.85$; hence, a second-order phase transition occurs. The transition is from the antiferromagnetic-3/2 ($AF_{3/2}$) phase to the P phase.

3.1.2. Internal energy, specific heat, entropy, and Helmholtz free energy

Figures 3*a*–*d* show the thermal behaviors of the internal energy, specific heat, entropy, and Helmoltz free energy of the spin-3/2 HIN system: Fig. 3 is obtained for $J_1 = 1.0$, $J_C = 1.0$, $J_S = 1.0$, and $D = 1.0$. Figure 3*a* shows the behavior of the internal energies. It expresses the continuity of the curvature at the critical temperature $T_C = 7.85$. The specific heat curves of the

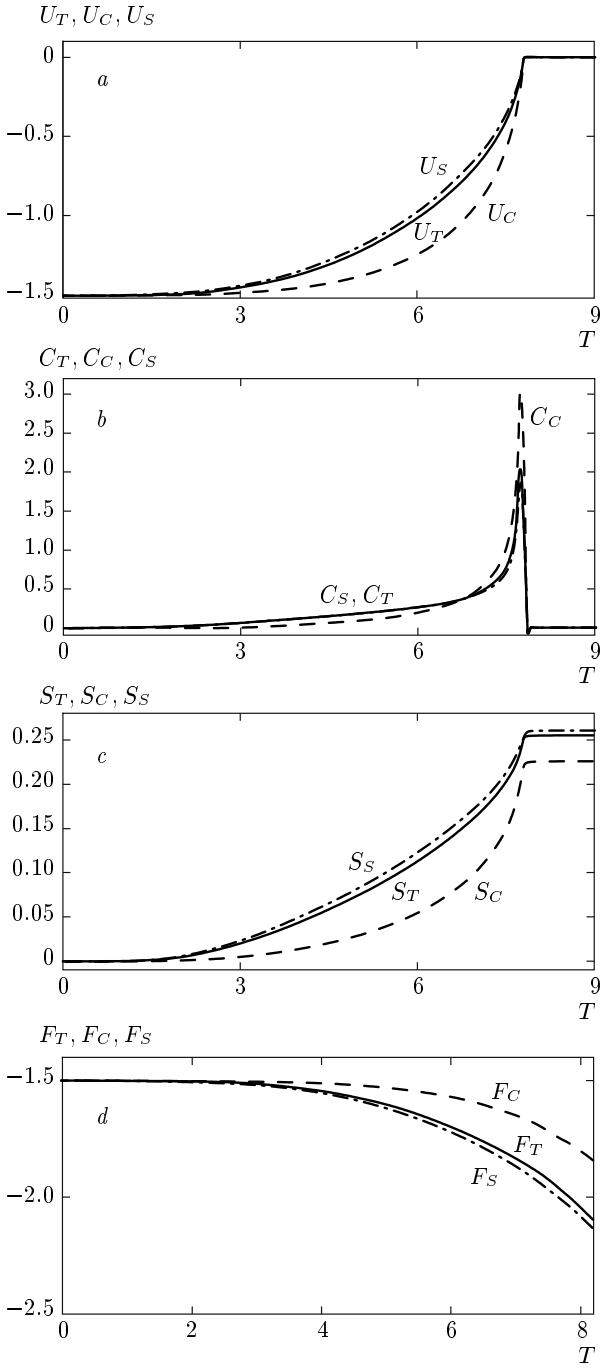

Fig. 3. For $J_1 = 1.0$, $J_C = 1.0$, $J_S = 1.0$, and $D = 1.0$ values, Figs. 3*a*–*d* respectively show thermal behaviors of the internal energy, specific heat, entropy, and Helmoltz free energy of the spin-3/2 HIN system. (Color online see arXiv:1406.6537)

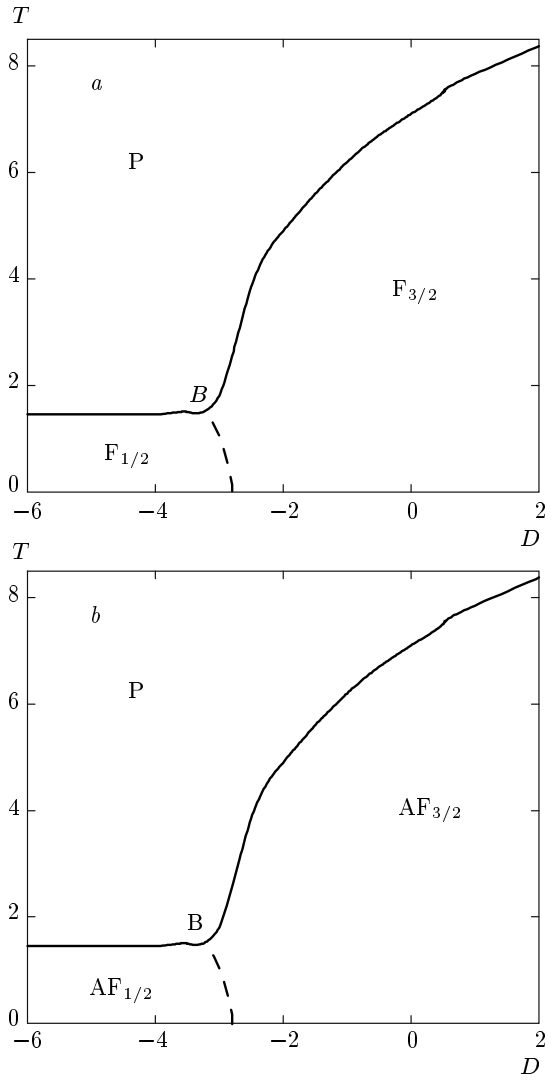

Fig. 4. The phase diagrams in the (D, T) plane of the spin-3/2 HIN system. Dashed and solid lines represent the respective first- and second-order phase transitions. (*a*) $J_1 = 1.0$, $J_C = 1.0$, and $J_S = 1.0$. (*b*) $J_1 = -1.0$, $J_C = 1.0$, and $J_S = 1.0$

system exhibit a second-order transition at $T_C = 7.85$ and rapidly decrease with increasing the temperature, as seen in Fig. 3*b*. Figure 3*c* illustrates the entropy of the spin-3/2 HIN system. As is known, entropy is not important at low temperatures and the ground-state energy corresponds to the free energy of the system. But, along with a temperature increase, in order to minimize its free energy the system tends to maximize its entropy. In this way, entropy becomes important. Finally, the Helmoltz free energy of the spin-3/2 HIN system is presented in Fig. 3*d*. It is evident from Eq. (13) that the free energy equals the internal energy at zero temperature. Free energies (total, core,

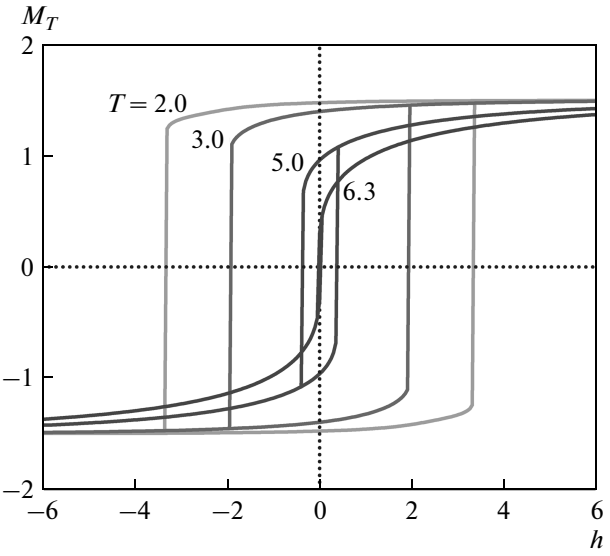

Fig. 5. Hysteresis behaviors of the spin-3/2 HIN system for $J_1 = 0.5$, $J_C = 1.0$, $J_S = 1.0$, and $D = 0.5$ and for various values of temperatures $T = 2.0$, 3.0, 5.0, 6.3. (Color online see arXiv:1406.6537)

and shell free energies) show a smooth decrease with increasing the temperature.

3.2. Phase diagrams

The phase diagrams of the spin-3/2 HIN system are presented in the (D, T) plane for both ferromagnetic and antiferromagnetic cases in Fig. 4. The solid and dashed lines represent the second- and first-order phase transitions. The system illustrates a special point, the double critical end point (B). Figure 4*a* is calculated for the ferromagnetic case ($J_1 > 0$) and $J_1 = 1.0$, $J_C = 1.0$, $J_S = 1.0$, and $D = 1.0$. The system shows ferromagnetic-3/2 ($F_{3/2}$), ferromagnetic-1/2 ($F_{1/2}$), and paramagnetic (P) fundamental phases as well as the B special point. For the very low values of D and T, the $F_{1/2}$ fundamental phase occurs in the system; for the low values of D and high values of the T, the P fundamental phase occurs in the system; for very low values of D and T, the $F_{3/2}$ fundamental phase occurs in the system. The $F_{1/2}$ and $F_{3/2}$ fundamental phases are separated from the paramagnetic phase by the B special point. The phase boundary is a second-order phase line except the boundary between the $F_{3/2}$ and $F_{1/2}$ phases, which is a first-order line. A first-order phase transition line occurs for low D values. Figure 4*b* is similar to Fig. 4*a* but differs from it: (i) the phase diagram is calculated for $J_1 = -1.0$, $J_C = 1.0$, $J_S = 1.0$, and $D = 1.0$. (ii) The $AF_{3/2}$ and $AF_{1/2}$ fundamental phases appear instead of the $F_{3/2}$ and $F_{1/2}$ fundamental phases.

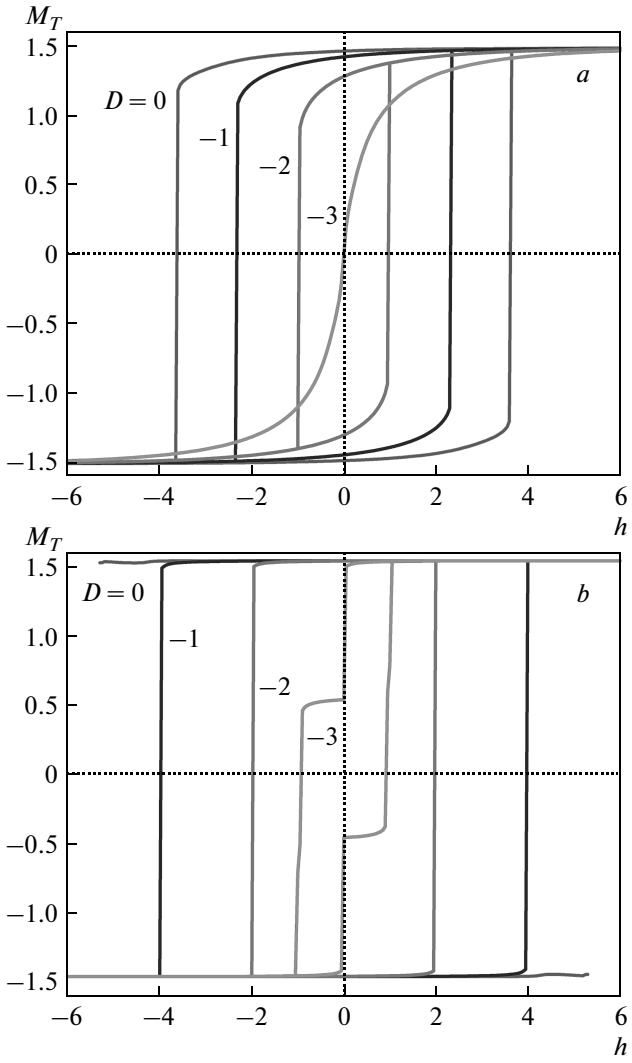

Fig. 6. The same as in Fig. 5, but for $J_1 = 1.0$, $J_C = 1.0$, $J_S = 1.0$, $T = 2.0$ (*a*), 0.5 (*b*), and $D = 0$, -1, -2, -3. (Fig. 6*a* color online see arXiv:1406.6537)

3.3. Hysteresis behaviors

In this subsection, we examine the effects of the temperature and crystal field on the hysteresis behaviors of a spin-3/2 HIN system.

3.3.1. The effects of temperature on the hysteresis behaviors

We illustrate the dependence of hysteresis loops of a spin-3/2 HIN system on the temperature ($T = 2.0$, 3.0, 5.0, and 6.3) for $J_1 = 0.5$, $J_C = 1.0$, $J_S = 1.0$, and $D = 0.5$ in Fig. 5. We see from this figure that the magnetization curves are symmetric for both positive and negative values of the external magnetic field. Moreover, for the temperature above the critical tem-

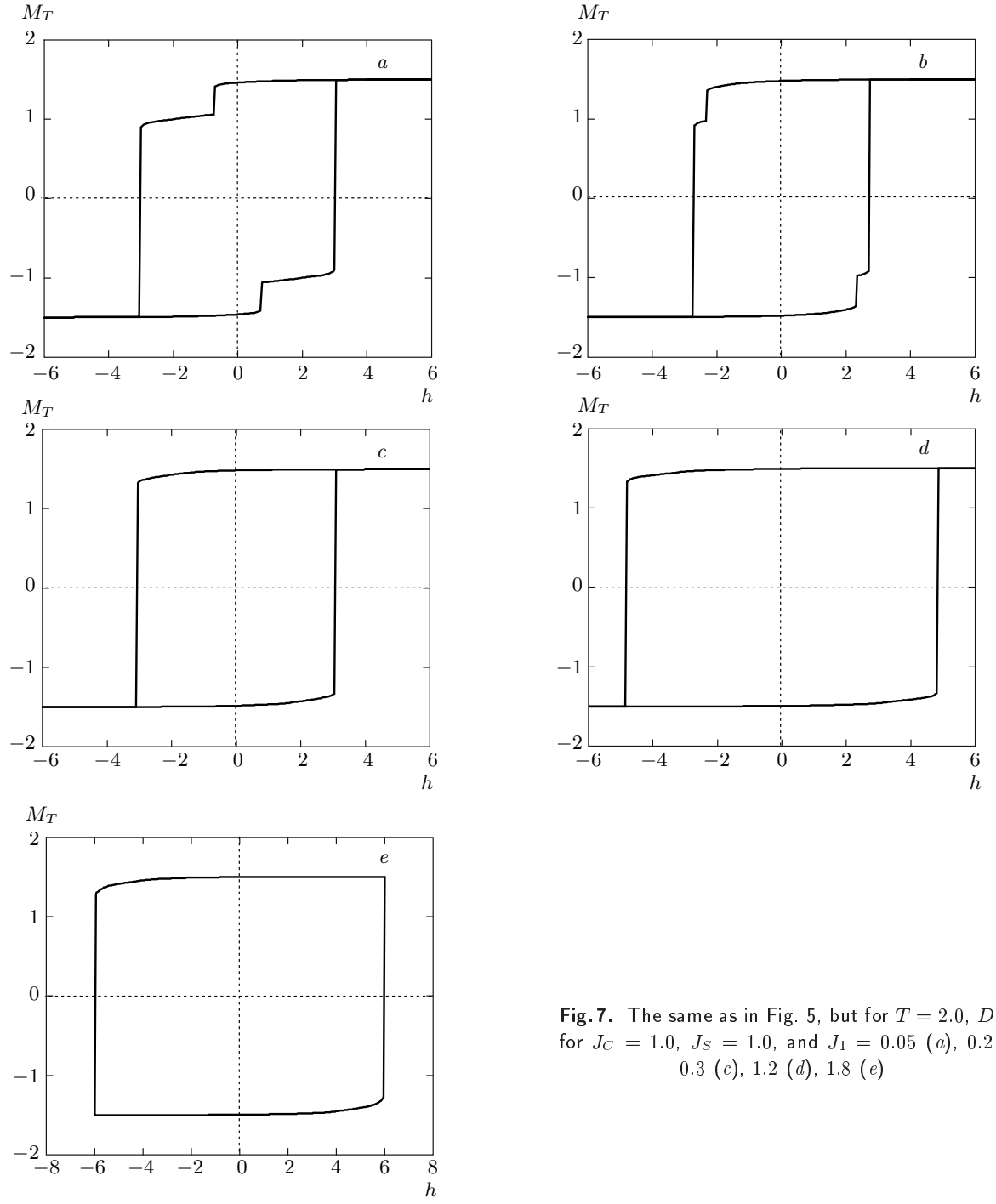

Fig. 7. The same as in Fig. 5, but for $T = 2.0$, $D = 0$ for $J_C = 1.0$, $J_S = 1.0$, and $J_1 = 0.05$ (a), 0.2 (b), 0.3 (c), 1.2 (d), 1.8 (e)

perature $T_C = 6.15$, we can see that the hysteresis loops disappear. Similar hysteresis loop behaviors have been observed in the random-field Ising model [52]. Furthermore, with increasing the temperature, the hysteresis loops decrease, and these results are consistent with some theoretical studies [53–55].

3.3.2. The effects of single-ion anisotropy on the hysteresis behaviors

Figure 6 shows the influence of the single-ion anisotropy on hysteresis. Figure 6a is plotted for $J_1 = 1.0$, $J_C = 1.0$, $J_S = 1.0$, and $T = 2.0$ fixed values, and $D = 0$, -1, -2, and -3 single-ion anisotropy val-

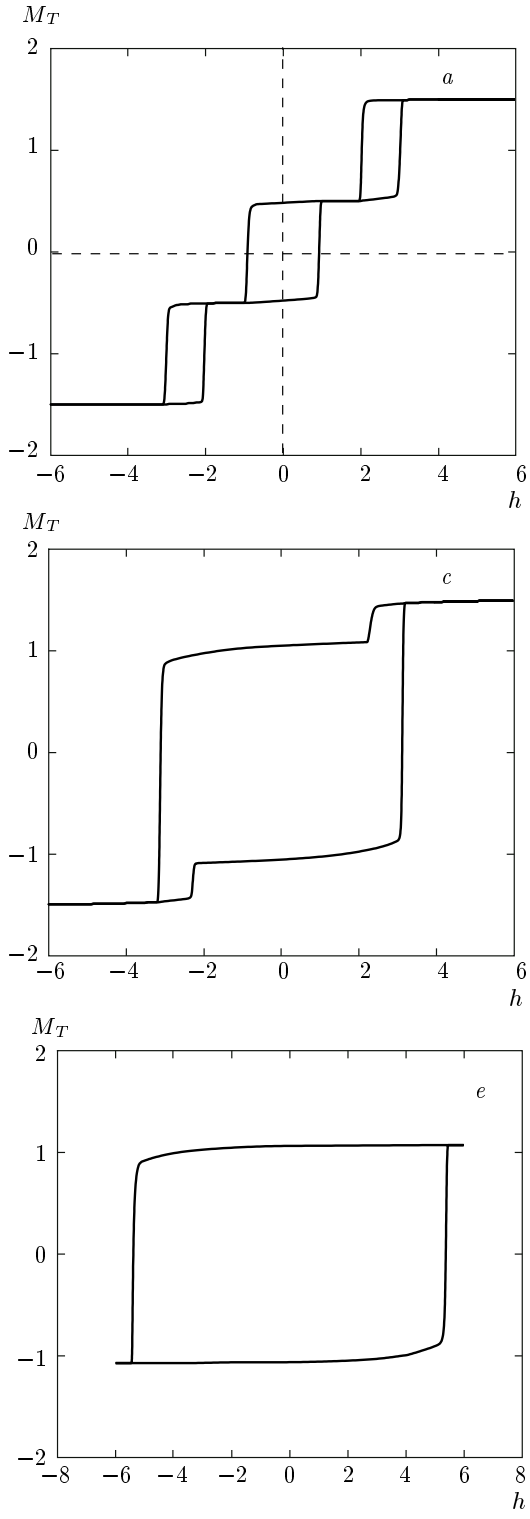

Fig. 8. The same as in Fig. 5, but for $T = 2.0$, $D = 0$ for $J_C = 1.0$, $J_S = 1.0$, and $J_1 = -0.05$ (a), -0.2 (b), -0.3 (c), -1.2 (d), -1.8 (e)

ues. We can see that with the decrease in the single-ion anisotropy, the hysteresis loop area narrows and the system exhibits only one hysteresis loop. These facts are clearly seen in Fig. 6, and the results are consistent with some theoretical models [46–48]. On the other hand, Fig. 6*b* is calculated for $J_1 = 1.0$, $J_C = 1.0$, $J_S = 1.0$, and $T = 0.5$ fixed values, and $D = 0$, -1, -2, and -3 single-ion anisotropy values. We can see that with the decrease in the single-ion anisotropy, the hysteresis loop area narrows. With the decrease in single-ion anisotropy, at $D = -3.0$, one hysteresis loop turns into a double hysteresis loops. Theoretically, similar result have been observed a spin-3/2 cylindrical Ising nanotube system [32].

3.3.3. The effect of core/shell interfacial coupling on the hysteresis

We present the core/shell interfacial coupling dependence of the hysteresis loops of a spin-3/2 HIN system at $T = 2.0$, $D = 0$ for $J_S = 1.0$, $J_C = 1.0$, and $J_1 = 0.05$, 0.2, 0.3, 1.2, and 1.8 in Fig. 7. The hysteresis consists of double loops in Figs. 7*a* and 7*b*. Theoretically, similar result have been observed for a spin-3/2 cylindrical Ising nanotube system [34]. On the other hand, we can see that when the core/shell interfacial coupling constant is large, the system always shows one loop, seen in Figs. 7*c–e*. We can see that as the core/shell interfacial coupling increases, the hysteresis behavior changes and the hysteresis loop area increases. This fact is clearly seen from Figs. 7*a–e*. We also obtained the hysteresis loops for the antiferromagnetic case in Fig. 8, for $T = 2.0$, $D = 0$, $J_C = 1.0$, $J_S = 1.0$, and $J_1 = -0.05$, -0.2, -0.3, -1.2, and -1.8. Figure 8*a* displays triple hysteresis loops for $r = -0.05$. As r decreases, the triple hysteresis loops first turn into double loops, then into a single hysteresis loop as seen in Figs. 8*a–e*. Theoretically, similar result have been observed for a spin-3/2 cylindrical Ising nanotube system [34].

4. SUMMARY AND CONCLUSION

By utilizing the effective field theory with correlations, we studied magnetic properties such as magnetizations, internal energy, specific heat, entropy, Helmholtz free energy, and phase diagrams of a spin-3/2 Blume–Capel model on a HIN with a core–shell structure. The effects of the Hamiltonian parameters on hysteresis behaviors are investigated in detail. The obtained results are compared with some theoretical results and a qualitatively good agreement is found.

We compared the results with the results of the one-dimensional Blume–Capel model calculation [56] and found that the one-dimensional Blume–Capel model exhibits only a second-order phase transition. On the other hand, the spin-3/2 HIN system exhibits both first- and second-order phase transitions. Moreover, the comparison of results with the magnetic properties of the spin-3/2 Blume–Capel model on a HIN with a core-shell structure and the magnetic properties of the one-dimensional spin-1/2 Ising system with a core-shell structure [39] can be summarized as follows. (1) The spin-1/2 Ising system only exhibits a second-order phase transition and does not exhibit a first-order phase transition, but the spin-3/2 HIN system shows both first- and second-order phase transitions. (2) The spin-1/2 Ising system exhibits two loops, but the spin-3/2 one shows there loops. (3) The spin-3/2 HIN system displays ferromagnetic-1/2, ferromagnetic-3/2, antiferromagnetic-1/2, antiferromagnetic-3/2, and paramagnetic fundamental phases, but the spin-1/2 Ising system exhibits only ferromagnetic, antiferromagnetic, and paramagnetic fundamental phases. Therefore, we can conclude that the spin-3/2 HIN system gives richer and more interesting magnetic properties than the spin-1/2 Ising system does.

Finally, we hope that our detailed theoretical investigations may stimulate further studies of the magnetic properties of nanoparticles systems, and it will also motivate researchers to investigate the behaviors in real nanostructured materials.

REFERENCES

1. M. Blume, Phys. Rev. **143**, 517 (1966).
2. H. W. Capel, Physica (Utr.) **32**, 966 (1966).
3. J. Sivardière and M. Blume, Phys. Rev. B **5**, 1126 (1972).
4. A. H. Cooke, D. M. Martin, and M. R. Wells, J. Phys. (Paris), Colloq. **32**, C1-488 (1971).
5. A. H. Cooke, D. M. Martin, and M. R. Wells, Sol. St. Comm. **9**, 519 (1971).
6. S. Krinsky and D. Mukamel, Phys. Rev. B **11**, 399 (1975).
7. T. Kaneyoshi and M. Jaščur, Phys. Rev. B **46**, 3374 (1992).

8. T. Kaneyoshi and M. Jaščur, Physica B **179**, 317 (1992).

9. L. Peliti and M. Saber, Phys. Stat. Sol. B **195**, 537 (1996).

10. A. Yiğit and E. Albayrak, Chin. Phys. B **22**, 100508 (2013).

11. A. Bakchich and M. El Bouziani, J. Phys.: Condens. Matter **13**, 91 (2001).

12. M. Žukovič and M. Jaščur, J. Magn. Magn. Mater. **354**, 272 (2014).

13. N. Tahiri, H. Ez-Zahraouy, and A. Benyoussef, Physica A **388**, 3426 (2009).

14. M. El Bouziani and A. Gaye, Physica A **392**, 2643 (2013).

15. N. Tahiri, H. Ez-Zahraouy, and A. Benyoussef, J. Supercond. Nov. Magn. **26**, 3143 (2013).

16. O. Baran and R. Levitskii, J. Magn. Magn. Mater. **324**, 3778 (2012).

17. O. Baran and R. Levitskii, Physica B **408**, 88 (2013).

18. T. Kaneyoshi, Sol. St. Comm. **151**, 1528 (2011).

19. T. Kaneyoshi, Phys. Stat. Sol. B **248**, 250 (2011).

20. C. D. Wang, Z. Z. Lu, W. X. Yuan, S. Y. Kwok, and B. H. Teng, Phys. Lett. A **375**, 3405 (2011).

21. N. Şarlı and M. Keskin, Sol. St. Comm. **152**, 354 (2012).

22. W. Jiang, H. Guan, Z. Wang, and A. Guo, Physica B **407**, 378 (2012).

23. T. Kaneyoshi, Sol. St. Comm. **152**, 883 (2012).

24. S. Bouhou, I. Essaoudi, A. Ainane, M. Saber, F. Dujardin, and J. J. de Miguel, J. Magn. Magn. Mater. **324**, 2434 (2012).

25. Y. Kocakaplan and E. Kantar, Chin. Phys. B **230**, 46801 (2014).

26. E. Kantar, B. Deviren, and M. Keskin, Eur. Phys. J. B **86**, 420 (2014).

27. A. Zaim, M. Kerouad, and Y. El Amraoui, J. Magn. Magn. Mater. **321**, 1083 (2009).

28. M. Ertaş and Y. Kocakaplan, Phys. Lett. A **378**, 845 (2014).

29. B. Deviren, M. Ertaş, and M. Keskin, Phys. Scripta **85**, 055001 (2012).

30. M. Ertaş and E. Kantar, Phase Transitions **88**, 567 (2015).

31. E. Kantar and M. Ertaş, Superlatt. Microstruct. **75**, 831 (2014).

32. E. Vatansever and H. Polat, J. Magn. Magn. Mater. **343**, 221 (2013).

33. Y. Yüksel, E. Vatansever, and H. Polat, J. Phys.: Condens. Matter **24**, 436004 (2012).

34. Y. Kocakaplan and M. Keskin, J. Appl. Phys. **116**, 093904 (2014).

35. T. Kaneyoshi, Sol. St. Comm. **152**, 1686 (2012).

36. T. Kaneyoshi, Physica B **407**, 4358 (2012).

37. Ü. Akıncı, J. Magn. Magn. Mater. **329**, 178 (2012).

38. T. Kaneyoshi, Phase Transitions **85**, 264 (2012).

39. N. Şarlı, Physica E **63**, 324 (2014).

40. H. B. Callen, Phys. Lett. **4**, 161 (1963).

41. T. Kaneyoshi, J. Phys. Soc. Jpn. **56**, 2675 (1987).

42. T. Kaneyoshi, Physica A **153**, 556 (1988).

43. Z. Y. Li and T. Kaneyoshi, Phys. Rev. B **37**, 7785 (1988).

44. T. Kaneyoshi, Sol. St. Comm. **70**, 975 (1989).

45. T. Kaneyoshi, J. Magn. Magn. Mater. **92**, 59 (1990).

46. T. Kaneyoshi, Physica A **205**, 677 (1994).

47. R. Honmura and T. Kaneyoshi, J. Phys. C: Sol. St. Phys. **12**, 3979 (1979).

48. T. Kaneyoshi, I. P. Fitipaldi, R. Honmura, and T. Manabe, Phys. Rev. B **29**, 481 (1981).

49. F. Zernike, Physica **7**, 565 (1940).

50. T. Kaneyoshi and H. Beyer, J. Phys. Soc. Jpn. **49**, 1306 (1980).

51. T. Kaneyoshi, R. Honmura, I. Tamura, and E. F. Sarmento, Phys. Rev. B **29**, 5121 (1984).

52. P. Shukla and R. S. Kharwanlang, Phys. Rev. B **83**, 011121 (2011).

53. E. Kantar and M. Ertaş, Sol. St. Comm. **188**, 71 (2014).

54. Ò. Iglesias and A. Labarta, Phys. Rev. B **63**, 184416 (2001).

55. Ò. Iglesias and A. Labarta, Physica B **343**, 286 (2004).

56. M. Jasčur and T. Kaneyoshi, Phys. Stat. Sol. (b) **174**, 537 (1992).